Tuning the topology of p-wave superconductivity in an analytically solvable two-band model

Haiping Hu, 1,2 Erhai Zhao, 1 and Indubala I. Satija 1 Department of Physics and Astronomy, George Mason University, Fairfax, Virginia 22030, USA 2 Department of Physics and Astronomy, University of Pittsburgh, Pennsylvania 15260, USA

(Received 30 September 2020; revised 8 December 2020; accepted 9 December 2020; published 24 December 2020)

We introduce and solve a two-band model of spinless fermions with p_x -wave pairing on a square lattice. The model reduces to the well-known extended Harper-Hofstadter model with half-flux quanta per plaquette and weakly coupled Kitaev chains in two respective limits. We show that its phase diagram contains a topologically nontrivial weak pairing phase as well as a trivial strong pairing phase as the ratio of the pairing amplitude and hopping is tuned. Introducing periodic driving to the model, we observe a cascade of Floquet phases with well defined quasienergy gaps and featuring chiral Majorana edge modes at the zero or π gap or both. Dynamical topological invariants are obtained to characterize each phase and to explain the emergence of edge modes in the anomalous phase where all the quasienergy bands have zero Chern number. The analytical solution is achieved by exploiting a generalized mirror symmetry of the model, so that the effective Hamiltonian is decomposed into that of spin-1/2 in magnetic field, and the loop unitary operator becomes spin rotations. We further show the dynamical invariants manifest as the Hopf linking numbers.

DOI: 10.1103/PhysRevB.102.235156

I. INTRODUCTION

Classification of the electronic wave functions according to their topological characteristics offers fresh insights about band insulators and superconductors described by Bogoliubov-de Gennes (BdG) mean-field Hamiltonians [1,2]. In two dimensions (2D), integer quantum Hall insulators and spinless $p_x \pm i p_y$ superconductors are two well-known examples of topological phases of matter characterized by an integer (\mathbb{Z}) invariant, e.g., the Chern number. A topologically nontrivial bulk gives rise to edge modes within the energy gap localized at the sample boundary. More specifically, the total number of chiral edge states (the net chirality) for a given gap equals to the total Chern number of all the bands below the gap. These edge states are protected against imperfections, e.g., disorder, as long as certain underlying symmetries of the systems are preserved. For example, the $p_x + ip_y$ superconductor has particle-hole symmetry and belongs to class D in the Altland-Zirnbauer symmetry classes [3–5]. Its simplest, single-band model has two phases, the strong pairing phase which is topological trivial with Chern number 0, and the topological nontrivial weak pairing phase which has Chern number 1 [6]. The edge excitations in the weak pairing phase are chiral Majorana fermions, i.e., their creation operators γ_{k}^{\dagger} satisfy $\gamma_k^{\dagger} = \gamma_{-k}$, where k is the momentum along the edge direction. And at each vortex core, there is localized Majorana zero mode, $\gamma_0^{\dagger} = \gamma_0$, which obeys non-Abelian statistics [7,8].

In this paper, we consider a two-band model of spinless p_x -wave superconductor in 2D. On one hand, our model reduces to the extended Harper-Hofstadter model [9,10] at π flux for vanishing superconducting order parameter, $\Delta \rightarrow 0$. On the other hand, it reduces to the one-dimensional Kitaev chain [11] if the hoppings along the y and diagonal

direction are turned off. Overall, it incorporates the competition between the band topology, inherited from the familiar integer quantum Hall effect, and p-wave superconductivity. Our main motivation is to explore its rich phases as the parameters of the model are varied and when the model is time-periodically driven. For the static system, we find a weak pairing phase with Chern number 2 that is similar to (but different from) the $p_x + ip_y$ state despite the pairing symmetry is p_x -wave, and a strong pairing phase that is topologically trivial and can be viewed as stacked Kitaev chains. Previously, there have been several works on the coupled-wire constructions of 2D topological superconductors [12–14]. Our model here differs in the hopping patterns as well as the pairing symmetry. For the driven (Floquet) system, however, we discover a myriad of new Floquet phases that feature zero and π chiral Majorana edge modes. These phases are characterized not only by the Chern numbers of the bands, but also the threewinding numbers of the unitary evolution operators. Thus, this two-band (the number of bands at positive energies) model enriches our understanding of topological superconductivity in 2D in and out of equilibrium, beyond the well known one-band model of $p_x + ip_y$ superconductivity.

Despite its apparent complexity relative to the single-band model, we show that this model can be solved analytically for both the static and driven (periodically kicked) cases. This is achieved by exploiting a generalized "mirror" symmetry, which leads to the decomposition of the 4×4 BdG Hamiltonian H into the direct sum of two 2×2 Hamiltonians in the mirror subspace labeled by \pm , $H=H_+\oplus H_-$. In other words, the problem reduces to that of a spin in a momentum-dependent magnetic field described by a Hamiltonian of the form $-\mathbf{B}_{\pm}(\mathbf{k})\cdot\boldsymbol{\sigma}$. The decomposition not only greatly simplifies the algebra, but also provides an intuitive picture for all the

topological properties, including the Chern number and winding number. It also leads to the definition of mirror-graded Chern numbers. Furthermore, we show that the nontrivial dynamical topology of the driven model manifests as Hopf links in the (\mathbf{k}, t) space. These appealing analytical and topological properties form the second motivation to introduce our model. Once Kitaev chain is realized in experiments, coupling them together and control the transverse hopping with the help of a synthetic magnetic field will naturally lead to our model. We stress that our main goal here is *not* to propose a model that can be readily realized in experiments. Rather, the toy model is introduced to understand to what extent the topological properties can be, in principle, tuned for a spinless p-wave superconductor in 2D while keeping the problem analytically tractable.

The paper is organized as follows. In Sec. II, we introduce the model, analyze the BdG Hamiltonian in momentum space, and discuss its decomposition in the eigenspace of the mirror symmetry. In Sec. III, we solve the static model to obtain its phase diagram and discuss the topological invariants of each phase (e.g., mirror-graded Chern numbers, the total Chern number) and the corresponding chiral Majorana edge states. We solve the periodically kicked model in Sec. IV and discuss the Floquet phases, their dynamical invariants, and edge modes in the zero and π gap. An alternative interpretation of the dynamical invariant is presented from the perspective of Hopf links. Section V discusses the implications of our results.

II. MODEL

Consider spinless fermions on a square lattice in two dimensions described by the following tight-binding Hamiltonian:

$$H_{s} = -\sum_{r} \left[J_{x} c_{r+\hat{x}}^{\dagger} c_{r} + J_{y} e^{i2n\pi\phi} c_{r+\hat{y}}^{\dagger} c_{r} \right.$$

$$\left. + J_{d} e^{i(n+\frac{1}{2})2\pi\phi} c_{r+\hat{x}+\hat{y}}^{\dagger} c_{r} + J_{d} e^{i(n-\frac{1}{2})2\pi\phi} c_{r-\hat{x}+\hat{y}}^{\dagger} c_{r} \right.$$

$$\left. + \Delta c_{r+\hat{x}}^{\dagger} c_{r}^{\dagger} + \text{H.c.} \right]. \tag{1}$$

Here, $\mathbf{r} = n\hat{x} + m\hat{y}$ labels the lattice sites with n, m being integers, c_r^{\dagger} creates a fermion at site r, and we have set the lattice spacing to be unity. The lattice configuration is schematically shown in Fig. 1(a). The parameters J_x , J_y , and J_d denote the hopping along the x, the y, and the lattice diagonal direction, respectively. There is a magnetic field along the z direction that gives rise to a magnetic flux ϕ per unit cell. In cold atom set ups using optical lattices, this can be achieved using artificial magnetic field [15]. In the Landau gauge, the vector potential $A_x = 0$ and $A_y = n\phi h/e$, where ϕ is the magnetic flux per plaquette of the square lattice measured in unit of flux quantum h/e. We will focus on $\phi = 1/2$, i.e., the case of π flux. The unit cell then consists of two adjacent plaquette aligned along the x direction. The magnetic Brillouin zone is $k_x \in [0, \pi]$ and $k_y \in [0, 2\pi]$. Finally, Δ is the p_x -wave Cooper pairing amplitude. We do not determine Δ self-consistently. Rather we treat it as a tunable parameter controlled by, for example, proximity effect with a nearby p_x -wave superconductor. For fixed m (a row of the lattice), the pairing bears the same form as the Kitaev chain [11]. In fact, the Hamiltonian (1) can be viewed as Kitaev chains extending in the x direction

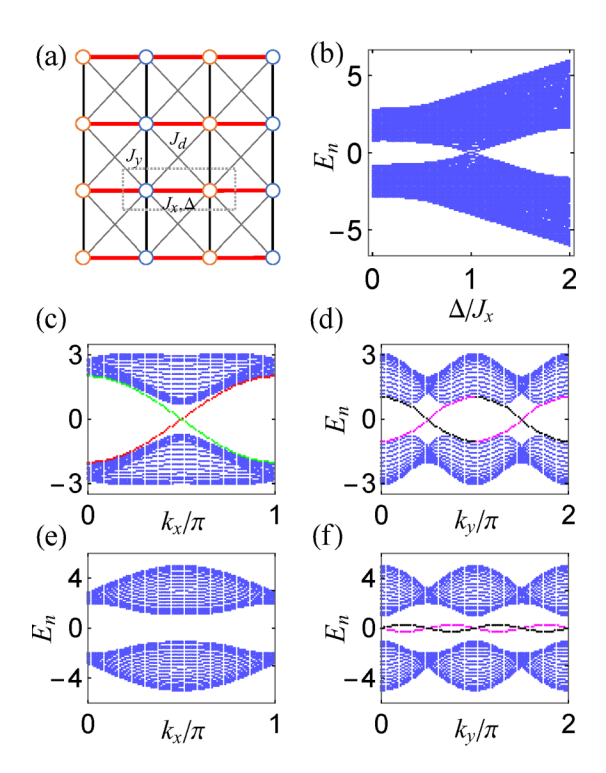


FIG. 1. (a) Schematics of the two-dimensional lattice and the model Hamiltonian (1). For half flux quantum per plaquette (ϕ = 1/2), each unit cell (the dotted box) contains two lattice sites (blue and orange circles). The hopping strengths along the x, y and diagonal directions are J_x , J_y , and J_d , with their phases given in Eq. (1). Δ is the p_x wave pairing along the x direction. (b) Energy spectra of the static Hamiltonian (1) as Δ is varied. The topological transition between the weak pairing phase and strong pairing phase occurs at $\Delta = J_x$ where the gap closes. [(c) and (e)] Energy spectra of the static model in stripe geometry with y-open boundary. The number of unit cells along the y direction used in the numerics is $L_y = 20$. Note that each edge mode in (c) is twofold degenerate. The red/green dots label the boundary states at the lower/upper boundaries. [(d) and (f)] Energy spectra of the static model in stripe geometry with x-open boundary. The number of unit cells along the x direction is $L_x = 20$. The magenta/black dots label boundary states at the left/right boundaries. The blue dots label the bulk bands. For (c) and (d), $\Delta = 0.5J_x$; for (e) and (f), $\Delta = 1.5J_x$. Other parameters are $\alpha = 0.2$, $\lambda = 1$. Energy is in units of J_x .

and coupled by J_y and J_d hopping. We have assumed the chemical potential $\mu = 0$. And we will measure energy in units of J_x .

In the limit of $\Delta=0$, the model reduces to the Harper-Hofstadter model at flux π with diagonal hopping J_d [16,17], which induces a gap at energy E=0. The two-band model exhibits quantum Hall effect. For small finite Δ , we will show below that the system is a topological superconductor similar to the p_x+ip_y chiral superconductor. For large Δ , the system is topologically trivial. Thus model (1) describes the competition between these two phases separated by a topological transition. We will first focus on the static case in Sec. III, where J_y , etc. are constant parameters. Later in Sec. IV, we will consider J_y as function of time t, for example,

$$J_{y} \rightarrow J_{y}(t) = J_{y}T \sum_{\ell} \delta(t - \ell T),$$

while all other parameters are held constant. In other words, the system is periodically kicked with time period T [18]. This is an example of Floquet, or periodically driven, systems for which H(t) = H(t+T) [19,20].

The Hamiltonian appears simpler in momentum space. Since the H_s is cyclic in y, Fourier transform along the y direction gives the following effective 1D Hamiltonian (with energy in units of J_x) for given quasimomentum k_y :

$$H(k_{y}) = -\sum_{n} \left[J_{n} c_{n+1,k_{y}}^{\dagger} c_{n,k_{y}} + \tilde{\Delta} c_{n+1,k_{y}}^{\dagger} c_{n,-k_{y}}^{\dagger} + \text{H.c.} \right]$$

$$+ \sum_{n} \mu_{n} (c_{n,k_{y}}^{\dagger} c_{n,k_{y}} - 1/2), \qquad (2)$$

where we have introduced

$$J_n = 1 + 2\alpha \cos \left[2\pi \phi (n + 1/2) + k_v\right]$$

and

$$\mu_n = 2\lambda \cos(2\pi \phi n + k_y).$$

Here, the ratio $\lambda = J_y/J_x$ is the x-y hopping anisotropy, $\alpha = J_d/J_x$, and $\tilde{\Delta} = \Delta/J_x$. For π flux, label the two sites within the unit cell as A and B. More explicitly, even n corresponds to the A sites for which

$$\mu^A = 2\lambda \cos k_v$$
, $J^A = 1 - 2\alpha \sin k_v$.

For n odd, or B sites,

$$\mu^B = -2\lambda \cos k_v$$
, $J^B = 1 + 2\alpha \sin k_v$.

We then perform another Fourier transform along the x axis,

$$c_{j,A}^{\dagger} = \frac{1}{\sqrt{N}} \sum_{k_x} e^{ik_x 2j} c_{A,k_x}^{\dagger},$$

$$c_{j,B}^{\dagger} = \frac{1}{\sqrt{N}} \sum_{k} e^{ik_x (2j+1)} c_{B,k_x}^{\dagger},$$

where j labels the unit cell, and N is the total number of unit cells, and $k_x \in [0, \pi]$. Introduce Nambu spinor $\Psi_k = (c_{A,k}, c_{B,k}, c_{A,-k}^{\dagger}, c_{B,-k}^{\dagger})^T$, then the original Hamiltonian becomes

$$H_s = \frac{1}{2} \sum_{\mathbf{k}} \Psi_{\mathbf{k}}^{\dagger} H_{\text{BdG}}(\mathbf{k}) \Psi_{\mathbf{k}}.$$

The Bogoliubov-de Gennes (BdG) Hamiltonian can be expressed in compact form

$$H_{BdG}(\mathbf{k}) = -2\lambda \cos k_y \sigma_z \tau_z - 2 \cos k_x \sigma_x \tau_z + 4\alpha \sin k_x \sin k_y \sigma_y + 2\tilde{\Delta} \sin k_x \sigma_x \tau_y.$$
 (3)

Here the Pauli matrices τ_i (σ_j) are defined within the particle-hole (AB sublattice) space. Products such as $\sigma_x \tau_y$ are understood as direct product $\sigma_x \otimes \tau_y$ where \otimes is omitted for brevity. A main appeal of our model H_s is that in \mathbf{k} space, it has a nice form $H_{\text{BdG}}(\mathbf{k})$, which facilitates analytical analysis. It is clear that our main motivation here is to construct a simple model that contains the interplay of band topology and p-wave superconductivity and can reduce to well-known models in certain limits.

The BdG Hamiltonian is invariant under the transformation $\mathcal{O} = \sigma_y \tau_x$ which switches particle to hole and simultaneously

sublattice A to B,

$$[H_{\text{BdG}}(\mathbf{k}), \mathcal{O}] = 0.$$

We will refer to \mathcal{O} as a generalized "mirror" symmetry [21], or mirror symmetry for short. The \mathcal{O} symmetry includes a mirror reflection about the center of a bond along the x-direction that swaps the A and B sublattice sites. This symmetry will play an important role in the topological characterization below. Let V be the unitary transformation that diagonalizes \mathcal{O} , $V^{\dagger}\mathcal{O}V = -\tau_z$. In the eigenbasis of \mathcal{O} , the Hamiltonian is decomposed into the direct sum [22]

$$V^{\dagger}H_{\mathrm{BdG}}(\mathbf{k})V = H_{-}(\mathbf{k}) \oplus H_{+}(\mathbf{k}),$$

where

$$H_{\pm}(\mathbf{k}) = 2(\pm \lambda \cos k_y - \tilde{\Delta} \sin k_x)\sigma_z + 2\cos k_x\sigma_x$$

$$\pm 4\alpha \sin k_x \sin k_y\sigma_y \tag{4}$$

are 2×2 matrices, i.e., k-dependent spin 1/2 Hamiltonians. Here the subscript \pm labels the subspace where \mathcal{O} is diagonalized and has eigenvalue ± 1 , respectively. The systematic simplification from H_s to H_\pm enables us to solve for its eigenspectra and obtain its topological invariants.

III. PHASE DIAGRAM OF THE STATIC MODEL

To find the spectra of the static BdG Hamiltonian, we can express it in a 2×2 block form,

$$H_{\text{BdG}} = \begin{pmatrix} D+F & -iG\\ iG & -D+F \end{pmatrix}, \tag{5}$$

where

$$D = -2\lambda \cos k_y \sigma_z - 2 \cos k_x \sigma_x,$$

$$F = 4\alpha \sin k_x \sin k_y \sigma_y,$$

$$G = 2\tilde{\Delta} \sin k_x \sigma_x.$$

Its square takes a very simple form,

$$H_{\text{BdG}}^2 = 4 \left[a + b \begin{pmatrix} 0 & \sigma_{\text{y}} \\ \sigma_{\text{y}} & 0 \end{pmatrix} \right],\tag{6}$$

where

$$a = \cos^2 k_x + \lambda^2 \cos^2 k_y + 4\alpha^2 \sin^2 k_x \sin^2 k_y + \Delta^2 \sin^2 k_x,$$

$$b = 2\lambda \tilde{\Delta} \cos k_y \sin k_x.$$

Consequently, the eigenvalues E of H_{BdG} are simply $\pm E_{\pm}$ with $E_{\pm} = 2\sqrt{a \pm b}$ or explicitly,

$$E_{\pm} = 2\sqrt{\cos^2 k_x + (\lambda \cos k_y \mp \tilde{\Delta} \sin k_x)^2 + 4\alpha^2 \sin^2 k_x \sin^2 k_y}.$$
(7)

Alternatively, we can start directly from the spin 1/2 Hamiltonians $H_{\pm}(\mathbf{k})$ in Eq. (4) and arrive at Eq. (7) immediately. According to Eq. (7), at positive energies there are two overlapping bands $E_{\pm}(\mathbf{k})$, corresponding to H_{\pm} respectively. The other bands at negative energies are just the particle-hole reflection of those at E > 0. The positive and negative bands are separated by a gap as shown in Fig. 1(b).

The bulk gap closes when $\tilde{\Delta} = \lambda$. The gap closing occurs at two **k** points, $k_1 = (\pi/2, 0)$ and $k_2 = (\pi/2, \pi)$. This marks

TABLE I. Summary of the topological invariants, defined in the main text, of the static model in the weak pairing (WP) phase and strong pairing (SP) phase. Also shown are the characterization of their edge modes.

	\mathcal{C}_{+}	\mathcal{C}_{-}	С	Edge modes
$\tilde{\Delta} < \lambda \text{ (WP)}$	1	1	2	Chiral Majorana
$\tilde{\Delta} > \lambda \left(\text{SP} \right)^{\prime}$	0	0	0	Edge dependent

a quantum phase transition point that separates two gapped phases, a weak pairing (WP) phase at $\tilde{\Delta} < \lambda$ and strong pairing (SP) phase for $\tilde{\Delta} > \lambda$. These two phases are topologically distinct. Even though the two bands are overlapping in energy, thanks to the \mathcal{O} symmetry and the decomposition Eq. (4), we can define the Chern number \mathcal{C}_{\pm} in each mirror subspace, e.g., for the lower band $-E_{\pm}(\mathbf{k})$ of H_{\pm} , respectively [23]. The total Chern number is then

$$\mathcal{C} = \mathcal{C}_{+} + \mathcal{C}_{-}.$$

We find C = 2 for weak pairing phase, while C = 0 for the strong pairing phase. Define the mirror-graded Chern number,

$$C_m = \frac{C_+ - C_-}{2}.$$

For the weak pairing phase, we find $C_+ = C_- = 1$, while for the strong pairing phase, $C_+ = C_- = 0$. In both cases, $C_m = 0$. The transition from the weak pairing phase to the strong pairing phase is a topological phase transition where the total Chern number changes by -2. This is summarized in Table I below. The situation here differs from another model we studied earlier, where the strong pairing phase has C = 2 and $C_m = 1$ [22]. A nonzero value of C_m means the presence of counter-propagating (sometimes referred to as helical) Majorana edge modes protected by mirror symmetry.

The distinction between the WP and SP phase is reflected in their edge states as illustrated in Fig. 1. The weak pairing phase is a topological superconductor characterized by $C_{\pm} = 1$. It is analogous to the $p_x + ip_y$ state, albeit with C = 2. According to the bulk-edge correspondence, there are two chiral Majorana edge modes on the system boundary, see Figs. 1(c) and 1(d). Note that in Fig. 1(c), each edge mode (in color red or green) is two-fold degenerate, in consistency with C = 2. In contrast, the strong pairing phase is topologically trivial. It can still have edge states, but their existence depend on the details, e.g., the orientation of edge, and therefore is not topologically protected. More specifically, edge states are absent at the upper and lower edges as shown in Fig. 1(e), but they appear at the left and right edges as shown in Fig. 1(f).

The edge-dependent boundary modes in the strong pairing phase can be further understood by viewing the 2D lattice system as coupled Kitaev chains. In the limit of $J_y = J_d = 0$, each chain along the x direction is a p_x -wave superconductor described by Kitaev's model with $\mu = 0$, which hosts Majorana zero modes at the chain boundary, say at x = 0 and x = L. Small but finite J_y and J_d couple these zero modes to lift their degeneracy. As a result, for an x-open boundary, the in-gap edge modes acquire dispersion in the y direction but remain well separated from the bulk band, in agreement with the numerical results in Fig. 1(e). Note that in this case there

is no net current flow along the edge. For *y*-open boundaries, each chain is fully gapped and weak inter-chain coupling do not introduce any in-gap modes. Thus the strong pairing phase as stacked Kitaev chains is a weak topological phase, but not a genuine 2D topological superconductor. Its edge-dependent boundary modes are reminiscent of the 1D topology. For the weak pairing phase at $\tilde{\Delta} < \lambda$, one no longer can treat the interchain coupling as small, and the system is intrinsically two-dimensional.

IV. THE PERIODICALLY DRIVEN MODEL

Now we generalize the static model Eq. (1) to see if periodic driving [24–31] can induce new topological phases that differ from the weak and strong pairing phase above. To this end, we make the replacement

$$J_{\rm y} o J_{\rm y}(t) = J_{\rm y} T \sum_\ell \delta(t - \ell T)$$

in H_s , such that $H_s(t) = H_s(t+T)$. In this periodically kicked model, J_x , J_d , and Δ are all held constant, while the hopping J_y is turned on when time t is multiples of the kicking period T, $t = \ell T$ with ℓ an integer. For this particular kicking protocol, the time-averaged hopping strength within each driving period is J_y . Here for simplicity we focus on the case of kicking only the J_y term while keeping J_d constant. For more general kicking protocols, e.g., kicking both the J_y and J_d terms, our numerics indicates that while the parameter regions of topological phases have changed, the key qualitative features of Floquet topological phases and their dynamical characterization remain roughly the same. At each time instant, the system is described by $H_{\text{BdG}}(\mathbf{k},t)$, or equivalently its decomposition $H_{\pm}(\mathbf{k},t)$, obtained from Eq. (3) by replacement

$$\lambda \to \lambda(t) = \lambda T \sum_{\ell} \delta(t - \ell T).$$

Define the time evolution operator as usual,

$$U(\mathbf{k},t) = \mathcal{T}e^{-i\int_0^t H_{\text{BdG}}(\mathbf{k},t')dt'},$$

where \mathcal{T} denotes time ordering. In particular, $U(\mathbf{k}, T)$ is known as the Floquet operator. Its eigenvalues $e^{i\omega_n(\mathbf{k})T}$ yield the quasienergy band structure $\{\omega_n(\mathbf{k})\}$, where n is the band index and the quasienergy ω_n is defined modulo $2\pi/T$. Due to the \mathcal{O} symmetry, to find the eigenvalues of $U(\mathbf{k}, T)$, it is sufficient to consider the Floquet operator in the \pm subspace of \mathcal{O} ,

$$U_{\pm}(\mathbf{k}, T) = \mathcal{T}e^{-i\int_0^T H_{\pm}(\mathbf{k}, t')dt'}$$

$$= e^{\pm 2iT\lambda\cos k_y\sigma_z}e^{-iT(-2\tilde{\Delta}\sin k_x\sigma_z + 2\cos k_x\sigma_x \pm 4\alpha\sin k_x\sin k_y\sigma_y)}$$

The 2×2 unitary matrix consists of two successive spin rotations, $U_{\pm}=e^{-i\chi_2\sigma_z}e^{-i\chi_1(\hat{n}\cdot\boldsymbol{\sigma})}$ where

$$\chi_1 = T \sqrt{4 \cos^2 k_x + 16\alpha^2 \sin^2 k_x \sin^2 k_y + 4\tilde{\Delta}^2 \sin^2 k_x},$$

$$\chi_2 = \pm 2T\lambda \cos k_y,$$

$$n_x = 2T \cos k_x / \chi_1,$$
(8)

$$n_{v} = \pm 4T\alpha \sin k_{x} \sin k_{y} / \chi_{1}, \tag{9}$$

$$n_7 = 2T\tilde{\Delta}\sin k_x/\chi_1. \tag{10}$$

Here we have suppressed the subscript \pm in χ_2 and n_y for brevity. Combining the two rotations, after straightforward algebra, we find the effective Hamiltonian \mathscr{H}_{\pm} of the periodically kicked system. It has the form of spin 1/2 in fictitious magnetic field \mathbf{B}_{\pm} ,

$$U_{\pm}(\mathbf{k},T) = e^{-i\mathscr{H}_{\pm}T} \equiv e^{-i(\mathbf{B}_{\pm}\cdot\boldsymbol{\sigma})T}.$$

The magnitude of \mathbf{B}_{\pm} is nothing but the quasienergy, $\omega_{\pm} = B_{\pm}$ (the negative branch of the quasienergy spectrum is simply $-\omega_{\pm}$ due to particle-hole symmetry), and it is given by equation

$$\cos(\omega_{\pm}T) = \cos(\chi_1)\cos(\chi_2) - n_z\sin(\chi_1)\sin(\chi_2). \tag{11}$$

Explicitly, the vector \mathbf{B}_{\pm} is given by

$$\mathbf{B}_{\pm}T = \frac{\omega_{\pm}T}{\sin(\omega_{\pm}T)} [\sin \chi_1 (n_x \cos \chi_2 - n_y \sin \chi_2)\hat{x} + \sin \chi_1 (n_x \sin \chi_2 + n_y \cos \chi_2)\hat{y} + (n_z \sin \chi_1 \cos \chi_2 + \sin \chi_2 \cos \chi_1)\hat{z}].$$
 (12)

Now that each quasienergy band $\omega_{\pm}(\mathbf{k})$ is mapped to a spin 1/2 problem, its Chern number can be obtained for example by plotting $\mathbf{B}_{\pm}(\mathbf{k})$ for \mathbf{k} inside the Brillouin zone.

Note that the effective magnetic field \mathbf{B}_{\pm} is well behaved as $\omega_{\pm}T \to 0$ but diverges as $\omega_{\pm}T \to \pi$. Physically, the divergence of the \mathbf{B}_{\pm} field occurs when the π gap closes for the bulk quasienergy bands. After going through this critical point, the number of chiral edge modes at the π gap changes. Furthermore, we note that in the fast driving limit of $T \to 0$, we recover the static model discussed in the previous section. To see this, we expand the sines and cosines in Eq. (11) to the order of T^2 to obtain

$$\omega_{\pm}T \simeq \sqrt{\chi_1^2 + \chi_2^2 + \chi_1 \chi_2 n_z},$$

which agrees with the quasienergy spectrum of the static model given by Eq. (7).

The various phases of the periodically driven system can be revealed by graphing the bulk quasienergy spectrum as function of the parameters of the model. For example, Fig. 2 shows the quasienergy as the pairing amplitude Δ is varied for fixed driving period T. Compared to the static cases with only two distinct phases, periodic kicking induces a series of Floquet phases, each of which has a gap at quasienergy 0, or π/T , or both. The differences between these phases are reflected in their edge states. The extra gap at quasienergy π/T (known as the π gap) gives rise to the possibility of new types of chiral Majorana modes that are intrinsically dynamical in nature [32,33]. We will refer to the edge modes inside the π gap (zero gap) as π modes (zero modes). For small Δ , there are a pair of chiral Majorana modes traveling along each edge within the zero gap only, similar to the weak pairing phase of the static model, see Fig. 2(a). By increasing Δ , the quasienergy bands touch each other at the π gap at $\Delta \approx 0.6 J_x$. This marks a topological transition into a phase which has a pair of chiral Majorana modes at the zero gap as well as the π gap, as depicted in Fig. 2(b). As noted earlier, \mathbf{B}_{+} becomes ill-defined when the π gap closes, $\omega_{+}T = \pi$, accompanied by dramatic changes in the π -edge modes. With further increase of Δ , another gap closing occurs at $\Delta \approx J_x$

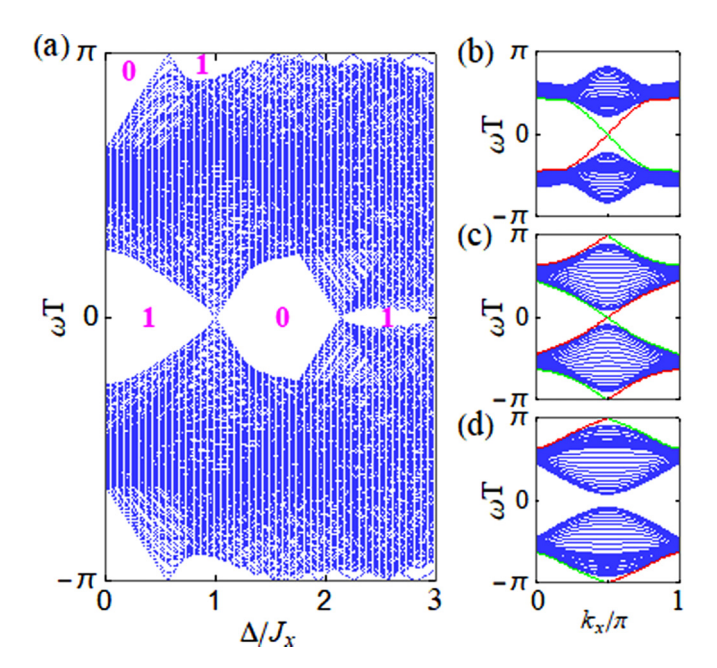


FIG. 2. Floquet phases of the periodically kicked model. (a) show the quasienergy spectrum ω_n as Δ is varied with fixed $\lambda=1$, $\alpha=0.2$, and T=1. The gaps are marked with the corresponding winding numbers W_0^+ and W_π^+ defined in the main text. (b), (c), and (d) show the quasienergies for strip geometry (with open y-boundary) at $\Delta=0.3J_x$, $0.8J_x$, and $1.1J_x$. In the static case, the first two values of Δ correspond to the weak pairing phase, while $\Delta=1.1J_x$ corresponds to the strong pairing phase. The red/green colors label the edge states near y=1 and $y=L_y$ edges; $L_y=60$. The blue dots label the bulk bands.

where the zero modes disappear. The system then enters into a Floquet phase characterized by π modes only, as shown in Fig. 2(c). This Floquet phase with π modes differs from the static strong pairing phase at the same Δ value. Yet another phase takes over for larger Δ , e.g., $\Delta \sim 2.5J_x$, which features chiral Majorana edge modes at the zero gap.

The intermediate phase for Δ between $0.6J_x$ and J_x is a dynamical anomalous phase [31]. Even though the Chern numbers of the quasienergy bands are zero, both zero and π modes are present. This example shows that Chern numbers alone are insufficient to capture the dynamical origin of the edge modes, as is the case in many Floquet phases. To correctly describe the bulk-edge correspondence in driven systems, we need to introduce dynamical topological invariants [32,33]. In our 2D model, the dynamical invariant is the threewinding number directly constructed from the time-evolution operator. The key concept here is the so-called loop unitary operator, also known as the return map [32]. The unitary evolution U(t) of a periodically driven system can be decomposed into a unitary loop $\tilde{U}(t)$ satisfying $\tilde{U}(0) = \tilde{U}(T) = I$ and the time evolution of a constant effective Hamiltonian ${\mathscr H}$ [34]. Explicitly, we can define $\mathcal{H}_{\epsilon} = i \log_{\epsilon} U(T)/T$ as well as the return map

$$\tilde{U}_{\epsilon}(t) = U(t)e^{i\mathcal{H}_{\epsilon}t}.$$
(13)

Here the subscript ϵ labels the quasienergy gap, and \log_{ϵ} denotes the logarithm with branch cut lying within gap ϵ

[31]. It is apparent from Eq. (13) that the topology of U(t) is carried by both \mathscr{H}_{ϵ} and $\tilde{U}_{\epsilon}(t)$. This point manifests the key difference between Floquet and static systems. It turns out that the number of chiral edge states at a chosen quasienergy gap ϵ is directly related to the phase-band closings [35] (also known as dynamical singularities) of the time-evolution operator in the entire driving period. As discussed above, the spectra of \mathscr{H}_{ϵ} give the quasienergy band structure, and each band carries a Chern number. The loop unitary U_{ϵ} defines a mapping from the space of (\mathbf{k}, t) , which is a three torus \mathbf{T}^3 , to a space of unitary matrices U(N). The corresponding topological invariant is the integer-valued winding number [31,33]

$$W_{\epsilon} = \frac{1}{24\pi^{2}} \int_{\mathbf{T}^{3}} dk_{x} dk_{y} dt \, \varepsilon^{\mu\nu\rho} \mathrm{Tr}$$

$$\times \left[(\tilde{U}_{\epsilon}^{-1} \partial_{\mu} \tilde{U}_{\epsilon}) (\tilde{U}_{\epsilon}^{-1} \partial_{\nu} \tilde{U}_{\epsilon}) (\tilde{U}_{\epsilon}^{-1} \partial_{\rho} \tilde{U}_{\epsilon}) \right], \qquad (14)$$

where $t \in [0, T]$, repeated indices $\mu, \nu, \rho \in \{k_x, k_y, t\}$ are summed over, and $\varepsilon^{\mu\nu\rho}$ is the Levi-Civita symbol. Geometrically, the three-winding number W_{ϵ} measures the total charge of the dynamical singularities of \tilde{U}_{ϵ} [35]. The stable singularities of \tilde{U}_{ϵ} take the form of Weyl points, i.e. isolated points in the space of (k_x, k_y, t) where the eigenphases of \tilde{U} , referred to as phase bands, touch each other, similar to those in a Weyl semimetal [35,36]. For an anomalous Floquet phase with finite W_{ϵ} , the dynamical singularities can not be smoothly deformed away to become a trivial phase with $W_{\epsilon} = 0$. One can further prove the following relation between the dynamical invariant W_{ϵ} and the Chern numbers of the Floquet bands between gap ϵ_2 and ϵ_1 [31]:

$$\sum_{\epsilon_1 < \epsilon_n < \epsilon_2} C_{\epsilon_n} = W_{\epsilon_2} - W_{\epsilon_1}. \tag{15}$$

The number of chiral edge states within a given gap ϵ is given by the invariant W_{ϵ} [31]. For phases that feature two gaps at quasienergy zero and π/T , respectively, the topological invariants (W_0, W_π) completely characterize the Floquet phase [32]. For our problem, due to the \mathcal{O} symmetry, U, \tilde{U} and \mathscr{H} can all be decomposed into the direct sum of 2×2 matrices in the eigenspace of \mathcal{O} . For example, the calculation of W_{ϵ}^+ only involves U(2) matrices. Then we can define $W_{\epsilon} = W_{\epsilon}^+ + W_{\epsilon}^-$ for $\epsilon = 0, \pi$.

Armed with the knowledge of W_{ϵ} , let us revisit the phase diagram in Fig. 2 from the viewpoint of dynamical invariants. For $0 < \Delta < 0.6J_x$, $W_0^{\pm} = 1$ and $W_{\pi}^{\pm} = 0$, which is in agreement of having a pair of chiral Majorana edge mode in the zero gap. For $0.6J_x < \Delta < J_x$, $W_0^{\pm} = 1$ and $W_{\pi}^{\pm} = 1$. Correspondingly, edge modes are visible in both gaps, and the Chern numbers vanish in accordance to Eq. (15). And finally for $J_x < \Delta < 1.5J_x$, $W_0^{\pm} = 0$, $W_{\pi}^{\pm} = 1$, so only π modes are present. The total Chern number (sum of contributions from both mirror subspaces) for the quasienergy bands below the zero gap are 2, 0, and -2, respectively, for the three phases above. We can clearly see that even when the Chern number of the bands are zero, edge states can still emerge. Such anomalous behavior is of dynamical origin and has no static counterparts.

Figure 3 further illustrates the rich phases of the system for various kicking period T. For small T, i.e., at high driving frequency, the system behaves like a static system in the

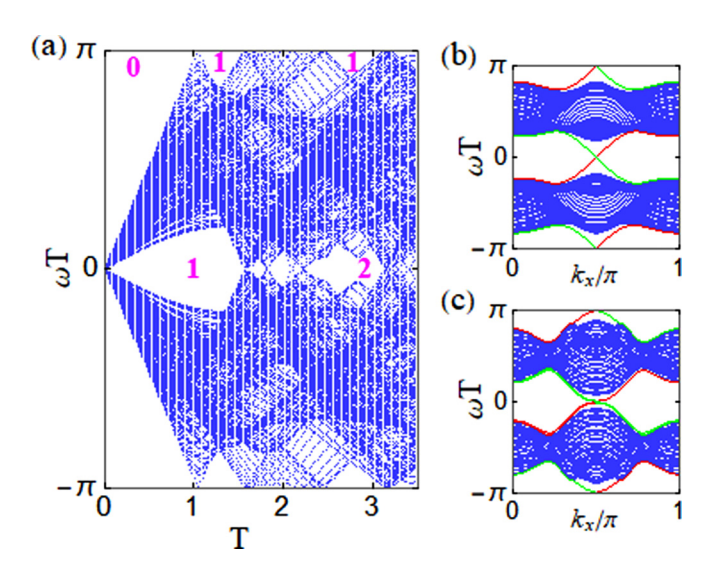


FIG. 3. The quasienergy spectrum (a) of the periodically kicked model as function of the driving period T with fixed $\lambda=1$, $\alpha=0.2$, and $\Delta=0.5J_x$. The major gaps are labeled with the corresponding winding numbers W_0^+ or W_π^+ . (b) [(c)] shows the edge state spectrum for strip geometry at T=1.3 (T=2.8), confirming the bulk-edge correspondence. The number of unit cells along the y direction is $L_y=60$.

weak pairing phase with a pair of chiral Majorana modes within the zero gap. With increasing T, the π -quasienergy gap closes around T=1 and then reopens. This ushers in a phase with a pair of chiral Majorana edge modes in the π gap, in addition to the edge modes within the zero gap, as depicted in Fig. 3(b). Its dynamical invariants are $W_0^{\pm}=W_{\pi}^{\pm}=1$, the same as the intermediate anomalous phase discussed in the preceding paragraph. Further increasing T leads the system to a gapless phase with no well defined quasienergy gaps. Even further increase in T, however, gives rise to a gapped phase around T=2.8 with $W_0^{\pm}=2$ and $W_{\pi}^{\pm}=1$. There are in total three pairs of chiral Majorana modes along each edge, two of which are degenerate within the zero gap, as depicted in Fig. 3(c).

The dynamical topology of the periodically kicked *p*-wave superconductor encoded in the time evolution operator $U_{\epsilon}(t)$ can be further understood from another geometric point of view [37,38]. Consider some arbitrary, topologically trivial initial state, for example $|\psi_0(\mathbf{k}, t=0)\rangle = (1,0)^T$. The time-evolved state generated by \tilde{U}_{ϵ} is a spinor,

$$|\psi_{\epsilon}^{\pm}(\mathbf{k},t)\rangle = \tilde{U}_{\epsilon}^{\pm}(\mathbf{k},t)|\psi_{0}(\mathbf{k},t=0)\rangle. \tag{16}$$

It defines a mapping from the three torus T^3 to the state space of spinors, the Bloch sphere S^2 . From homotopy point of view, this mapping is characterized by the linking invariant defined as follows [34,37–39]

$$\mathcal{L}_{\epsilon}^{\pm} = -\frac{1}{4\pi^2} \int_{\mathbb{T}^3} dk_x dk_y dt \; \varepsilon^{\mu\nu\rho} \psi_{\epsilon}^{\dagger} \partial_{\mu} \psi_{\epsilon} \partial_{\nu} \psi_{\epsilon}^{\dagger} \partial_{\rho} \psi_{\epsilon}, \quad (17)$$

with the partial derivative with respect to k_x , k_y and t and $\varepsilon^{\mu\nu\rho}$ the Levi-Civita symbol. In Eq. (17), we have suppressed the superscript \pm of ψ to avoid clutter. Note that the definition of above linking invariant is possible because the evolution is

time periodic, $\tilde{U}_{\epsilon}(t=0) = \tilde{U}_{\epsilon}(t=T) = I$, and the 4×4 BdG Hamiltonian can be decomposed into two 2×2 Hamiltonians, H_{\pm} . For our Floquet system, we can ignore the nontrivial cycles of the torus, which does not play a role here, and treat T^3 as three sphere S^3 [40–42]. The homotopy mapping above then reduces to the famed Hopf mapping in mathematics, and the homotopy invariant defined in Eq. (17) is nothing but the Hopf invariant $\pi_3(S^2) = \mathbb{Z}$.

Under the action of the loop unitary \tilde{U}_{ϵ} , for a chosen momentum-time value (k_x, k_y, t) , the initial state is transformed to a specific point on the Bloch sphere. Conversely, if we fix one specific point on the Bloch sphere, the preimage of the Hopf mapping will take the form of a closed trajectory in the 3D momentum-time space (if there is any). If we chose two distinct points on the Bloch sphere (the target states), their preimage trajectories, as two closed loops, will produce a linking pattern in the momentum-time space. The Hopf invariant is nothing but the linking number of the two curves, which is also intimately related to the geometric phase [43,44]. We note that this equation along with Eq. (15) is reminiscent of the CWF theorem in classical differential geometry for twisted space curves [43,44] whose topology is modeled by a thin ribbon. One can further show that the linking number of the preimages of any two points on the Bloch sphere is exactly the three-winding number defined earlier in Eq. (14) [38],

$$\mathcal{L}_{\epsilon}^{\pm} = W_{\epsilon}^{\pm}. \tag{18}$$

This equivalence provides an intuitive geometric picture of the dynamical topology of our kicked system. It also suggests a promising way for experimental detection of the dynamical topology by measuring the Hopf links, which were recently observed in quench dynamics using momentum-time resolved Bloch-state tomography [45–47].

The Hopf link characterization of our periodically kicked model is summarized in Fig. 4. Let us focus on the mirror subspace + (same result applies to the - subspace). An initial state at the north pole on the Bloch sphere will be "scattered" to points on the Bloch sphere under the evolution with the loop unitary. At $\Delta = 0.3$, the kicked system host edge modes only within the zero gap. Correspondingly, the preimage trajectories of the two distinct target states evolved by U_{π}^{+} are completely disjointed in the momentum-time space as depicted in Fig. 4(a), and their linking number is $\mathcal{L}_{\pi}^{+}=0$. In contrast, the preimages of U_0^+ form links with linking number $\mathcal{L}_0^+=1$ as depicted in Fig. 4(b). At $\Delta=0.8$, the kicked system host both 0-modes and π -modes. The system is in the dynamical anomalous phase. The preimage trajectories of both U_{π}^{+} and U_{0}^{+} are linked together, with linking number $\mathcal{L}_0^+ = \mathcal{L}_\pi^+ = 1$, as shown in Figs. 4(c) and 4(d), in consistency with their bulk winding number $W_0^+ = W_{\pi}^+ = 1$. We stress that the time-evolved spinor wave function is gauge dependent [recall $H_{BdG}(\mathbf{k})$ depends on the gauge choice], but the linking number is gauge invariant. For our gauge choice, it is most convenient to plot the preimages of time-evolved states in the extended Brillouin zone scheme, for example within the interval $k_x \in [0, 2\pi]$ as done in Fig. 4. In this way, the linking number can be easily counted. We note that different choices of the target states will result in different trajectories in the 3D (k_x, k_y, t) space. However, the linking number of the

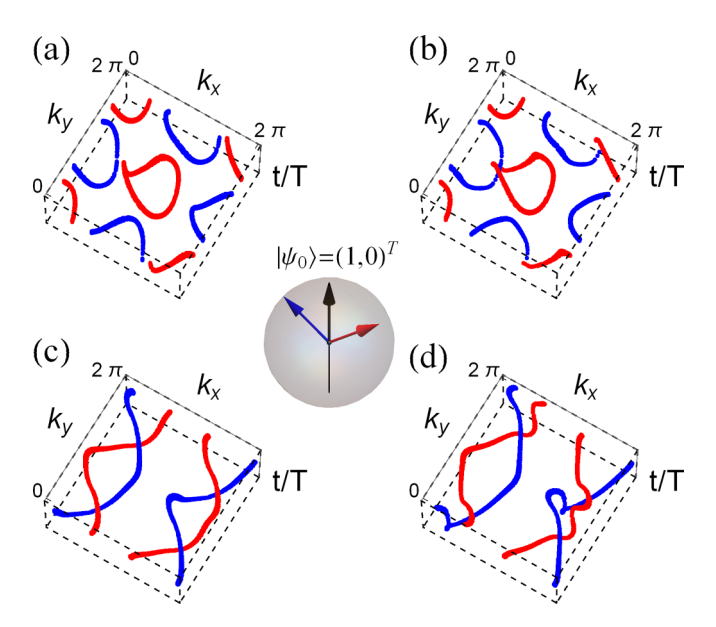


FIG. 4. Hopf links in the 3D momentum-time space as a characterization of bulk dynamical topology. (a) and (b) show the preimages of two chosen target states (red and blue arrows on the Bloch sphere, see the inset) under the evolution of \tilde{U}_{π}^{+} and \tilde{U}_{0}^{+} , respectively, for $\Delta=0.3J_x$. The Hopf linking number $\mathcal{L}_{\pi}^{\pm}=0$, $\mathcal{L}_{0}^{\pm}=1$. (c) and (d) show the results for $\Delta=0.8J_x$. Here the linking number $\mathcal{L}_{\pi}^{\pm}=1$, $\mathcal{L}_{0}^{\pm}=1$. Note that k_x is plotted from 0 to 2π . The middle inset gives the initial state $|\psi_0\rangle=(1,0)^T$ (black arrow) and two target states $|\psi_{blue}\rangle=\frac{1}{\sqrt{5}}(2,1)^T$ and $|\psi_{red}\rangle=\frac{1}{\sqrt{5}}(-2,1)^T$ (blue and red arrows) on the Bloch sphere. Other parameters are $\lambda=1$, $\alpha=0.2$ and T=1.

trajectories, which is a topological invariant and equals to the corresponding three-winding number, will remain the same.

V. DISCUSSIONS

It is well known that periodic driving offers a powerful technique to engineer the band topology of topological insulators. For example, in our previous work, we found a series of Floquet phases for the periodically kicked Harper-Hofstadter at π flux (but with no pairing), where the edge modes curiously take the simple form of cosine function in its dispersion [48]. We have also investigated periodically driven p-wave superconductors that consist of coupled Kitaev chains (but in the absence of magnetic flux or diagonal hopping), where chiral Majorana edge modes were found in the zero gap for a specially designed four-step driving [36]. Compared to these earlier studies, the model introduced here is more general and complex. But paradoxically, analytical solutions are possible by a consistent decomposition based on symmetry. The decomposition also greatly aids the visualization and computation of the Chern numbers and the three-winding numbers. Furthermore, it yields fresh insights by relating the dynamical topology to Hopf links. The topological invariants computed for each of the various Floquet phases accurately predict the edge modes in the quasienergy gap. In principle, our model can be realized via coupled Kitaev chains in solidstate systems, where the 1D (effective) p-wave topological superconductor has been demonstrated using semiconducting nanowires with spin-orbit coupling in proximity to an s-wave superconducting reservoir [49–51]. The Peierls phase in the hopping terms can be controlled by a perpendicular magnetic field. Alternatively, our model can also be potentially realized in ultracold dipolar Fermi gases, where the dipolar interaction gives rise to p_x -wave pairing if the dipoles are tilted toward the x direction so there is no need for proximity effect [36]. In addition, compared to solid-state setups, synthetic gauge fields are highly tunable in cold-atom systems. The main lesson learned from this theoretical toy model is that chiral Majorana edge modes, either static or dynamical (for example the π modes), is quite general and not confined to the $p_x \pm ip_y$ state. In particular, the π -Majorana fermions on the edge are

protected by dynamical invariants. This broadens the experimental options for manipulating chiral Majorana fermions for quantum gates or topological quantum computing [22,52]. We hope the technical approach presented here is useful for theoretical analysis of multiple-band superconductors that possess additional symmetries, and for visualization of the topological characteristics of other Floquet systems.

ACKNOWLEDGMENT

This work is supported by Air Force Office of Scientific Research Grant No. FA9550-16-1-0006 and National Science Foundation Grant No. PHY-1707484.

- [1] M. Z. Hasan and C. L. Kane, Rev. Mod. Phys. 82, 3045 (2010).
- [2] X.-L. Qi and S.-C. Zhang, Rev. Mod. Phys. 83, 1057 (2011).
- [3] A. Altland and M. R. Zirnbauer, Phys. Rev. B 55, 1142 (1997).
- [4] A. Kitaev, AIP Conf. Proc. 1134, 22 (2009).
- [5] A. P. Schnyder, S. Ryu, A. Furusaki, and A. W. W. Ludwig, Phys. Rev. B 78, 195125 (2008).
- [6] N. Read and D. Green, Phys. Rev. B 61, 10267 (2000).
- [7] D. A. Ivanov, Phys. Rev. Lett. 86, 268 (2001).
- [8] C. Nayak, S. H. Simon, A. Stern, M. Freedman, and S. Das Sarma, Rev. Mod. Phys. 80, 1083 (2008).
- [9] P. G. Harper, Proc. Phys. Soc., London, Sect. A 68, 874 (1955).
- [10] D. R. Hofstadter, Phys. Rev. B 14, 2239 (1976).
- [11] A. Y. Kitaev, Phys. Usp. 44, 131 (2001).
- [12] Z. Yan, R. Bi, and Z. Wang, Phys. Rev. Lett. 118, 147003 (2017).
- [13] F. Yang, V. Perrin, A. Petrescu, I. Garate, and K. Le Hur, Phys. Rev. B 101, 085116 (2020).
- [14] I. Seroussi, E. Berg, and Y. Oreg, Phys. Rev. B 89, 104523 (2014).
- [15] J. Dalibard, F. Gerbier, G. Juzeliūnas, and P. Öhberg, Rev. Mod. Phys. 83, 1523 (2011).
- [16] D. J. Thouless, Phys. Rev. B 28, 4272 (1983).
- [17] Y. Hatsugai and M. Kohmoto, Phys. Rev. B 42, 8282 (1990).
- [18] M. Lababidi, I. I. Satija, and E. Zhao, Phys. Rev. Lett. 112, 026805 (2014).
- [19] M. Bukov, L. D'Alessio, and A. Polkovnikov, Adv. Phys. 64, 139 (2015).
- [20] A. Eckardt, Rev. Mod. Phys. 89, 011004 (2017).
- [21] F. Zhang, C. L. Kane, and E. J. Mele, Phys. Rev. Lett. 111, 056403 (2013).
- [22] H. Hu, I. I. Satija, and E. Zhao, New J. Phys. 21, 123014 (2019).
- [23] K. Shiozaki and M. Sato, Phys. Rev. B 90, 165114 (2014).
- [24] T. Oka and H. Aoki, Phys. Rev. B 79, 081406(R) (2009).
- [25] N. H. Lindner, G. Refael, and V. Galitski, Nat. Phys. 7, 490 (2011).
- [26] T. Kitagawa, E. Berg, M. Rudner, and E. Demler, Phys. Rev. B 82, 235114 (2010).
- [27] N. H. Lindner, D. L. Bergman, G. Refael, and V. Galitski, Phys. Rev. B 87, 235131 (2013).
- [28] T. Kitagawa, T. Oka, A. Brataas, L. Fu, and E. Demler, Phys. Rev. B 84, 235108 (2011).

- [29] L. Jiang, T. Kitagawa, J. Alicea, A. R. Akhmerov, D. Pekker, G. Refael, J. I. Cirac, E. Demler, M. D. Lukin, and P. Zoller, Phys. Rev. Lett. 106, 220402 (2011).
- [30] Z. Gu, H. A. Fertig, D. P. Arovas, and A. Auerbach, Phys. Rev. Lett. **107**, 216601 (2011).
- [31] M. S. Rudner, N. H. Lindner, E. Berg, and M. Levin, Phys. Rev. X 3, 031005 (2013).
- [32] R. Roy and F. Harper, Phys. Rev. B 96, 155118 (2017).
- [33] S. Yao, Z. Yan, and Z. Wang, Phys. Rev. B 96, 195303 (2017).
- [34] H. Hu, C. Yang, and E. Zhao, Phys. Rev. B 101, 155131 (2020).
- [35] F. Nathan and M. S. Rudner, New J. Phys. 17, 125014 (2015).
- [36] E. Zhao, Zeitschrift für Naturforschung A 71, 883 (2016).
- [37] F. N. Ünal, A. Eckardt, and R.-J. Slager, Phys. Rev. Research 1, 022003(R) (2019).
- [38] H. Hu and E. Zhao, Phys. Rev. Lett. 124, 160402 (2020).
- [39] C. Wang, P. Zhang, X. Chen, J. Yu, and H. Zhai, Phys. Rev. Lett. **118**, 185701 (2017).
- [40] F. Wilczek and A. Zee, Phys. Rev. Lett. **51**, 2250 (1983).
- [41] J. E. Moore, Y. Ran, and X.-G. Wen, Phys. Rev. Lett. **101**, 186805 (2008).
- [42] D.-L. Deng, S.-T. Wang, C. Shen, and L.-M. Duan, Phys. Rev. B 88, 201105(R) (2013).
- [43] J. H. White, Am. J. Math. 91, 693 (1969).
- [44] R. Balakrishnan and I. I. Satija, arXiv:math-ph/0507039.
- [45] M. Tarnowski, F. N. Ünal, N. Fläschner, B. S. Rem, A. Eckardt, K. Sengstock, and C. Weitenberg, Nat. Commun. 10, 1728 (2019).
- [46] W. Sun, C.-R. Yi, B.-Z. Wang, W.-W. Zhang, B. C. Sanders, X.-T. Xu, Z.-Y. Wang, J. Schmiedmayer, Y. Deng, X.-J. Liu, S. Chen, and J.-W. Pan, Phys. Rev. Lett. 121, 250403 (2018).
- [47] C.-R. Yi, J.-L. Yu, W. Sun, X.-T. Xu, S. Chen, and J.-W. Pan, arXiv:1904.11656.
- [48] I. I. Satija and E. Zhao, Phys. Rev. B 94, 245128 (2016).
- [49] L. Rokhinson, X. Liu, and J. Furdyna, Nat. Phys. 8, 795 (2012).
- [50] V. Mourik, K. Zuo, S. M. Frolov, S. R. Plissard, E. P. A. M. Bakkers, and L. P. Kouwenhoven, Science 336, 1003 (2012).
- [51] A. Das, Y. Ronen, Y. Most, Y. Oreg, M. Heiblum, and H. Shtrikman, Nat. Phys. 8, 887 (2012).
- [52] B. Lian, X.-Q. Sun, A. Vaezi, X.-L. Qi, and S.-C. Zhang, Proc. Natl. Acad. Sci. USA 115, 10938 (2018).